Spontaneous Entrapment of Polynucleotides upon Electrostatic Interaction with Ethanol-Destabilized Cationic Liposomes

Norbert Maurer,* Kim F. Wong,* Holger Stark,† Lenore Louie,* Deirdre McIntosh,* Tabitha Wong,* Peter Scherrer,* Sean C. Semple,‡ and Pieter R. Cullis*‡

*Department of Biochemistry and Molecular Biology, University of British Columbia, Vancouver, British Columbia, Canada V6T 1Z3; †Institut für Molekularbiologie und Tumorforschung, Philips-Universität Marburg, D-35037 Marburg, Germany; and ‡Inex Pharmaceuticals Corporation, Burnaby, British Columbia, Canada V5J 5J8

ABSTRACT This study describes the effect of ethanol and the presence of poly(ethylene) glycol (PEG) lipids on the interaction of nucleotide-based polyelectrolytes with cationic liposomes. It is shown that preformed large unilamellar vesicles (LUVs) containing a cationic lipid and a PEG coating can be induced to entrap polynucleotides such as antisense oligonucleotides and plasmid DNA in the presence of ethanol. The interaction of the cationic liposomes with the polynucleotides leads to the formation of multilamellar liposomes ranging in size from 70 to 120 nm, only slightly bigger than the parent LUVs from which they originated. The degree of lamellarity as well as the size and polydispersity of the liposomes formed increases with increasing polynucleotide-to-lipid ratio. A direct correlation between the entrapment efficiency and the membrane-destabilizing effect of ethanol was observed. Although the morphology of the liposomes is still preserved at the ethanol concentrations used for entrapment (25–40%, v/v), entrapped low-molecular-weight solutes leak rapidly. In addition, lipids can flip-flop across the membrane and exchange rapidly between liposomes. Furthermore, there are indications that the interaction of the polynucleotides with the cationic liposomes in ethanol leads to formation of polynucleotide-cationic lipid domains, which act as adhesion points between liposomes. It is suggested that the spreading of this contact area leads to expulsion of PEG-ceramide and triggers processes that result in the formation of multilamellar systems with internalized polynucleotides. The high entrapment efficiencies achieved at high polyelectrolyte-to-lipid ratios and the small size and neutral character of these novel liposomal systems are of utility for liposomal delivery of macromolecular drugs.

INTRODUCTION

Liposomal formulations of genetic drugs such as antisense oligonucleotides and plasmid DNA are difficult to achieve (Maurer et al., 1999). The large size and highly charged nature of these molecules mitigates against the formation of small, neutral, serum-stable carriers, which are required to achieve the long circulation times necessary for efficient accumulation at disease sites. Furthermore, entrapment is very inefficient in the absence of interactions between the lipid components of the carrier and the nucleotide-based drugs. Complexes formed by electrostatic interactions between polynucleotides and cationic liposomes exhibit broad size distributions. These complexes efficiently transfect cells in vitro; however, in vivo their large size and positive charge triggers rapid clearance from the circulation (Felgner et al., 1987; Gao and Huang, 1995; Felgner, 1997; Chonn and Cullis, 1998; Tam et al., 2000). They can also be highly toxic (Tam et al., 2000). Therefore, substantial effort has been focused on constructing lipid-based carriers with improved characteristics.

Interaction of multivalent ions and polyelectrolytes with oppositely charged liposomes can result in phase separation and aggregation accompanied by structural transformations such as membrane rupture and fusion (Papahadjopoulos and Poste, 1975; Hope et al., 1983; Rand et al., 1985; Kachar et al., 1986; Lipowsky, 1991; Leckband et al., 1993; Sackmann, 1994; Mitrakos and Macdonald, 1996; Mok and Cullis, 1997; Macdonald et al., 1998). In the case of polynucleotide-cationic liposome complexes, size as well as structural features of complexes are determined by a delicate interplay between the ionic strength of the solution, the charge ratio, the overall concentrations of reactants, the kinetics of mixing, and liposome size and composition (Lasic, 1997; Xu et al., 1999). In general, the size of the complexes decreases when one of the components is present in excess so that the negative-to-positive charge ratio is much higher or lower than 1, at low ionic strength, upon rapid mixing, and at low overall concentrations of reactants ($\leq$1 mM lipid). Complexes are thermodynamically unstable and display a tendency to grow into larger aggregates over time, which may undergo further structural rearrangements (Radler et al., 1998). As a result, complexes typically have broad size distributions and are structurally heterogeneous. Structural features of complexes include clusters of aggregated liposomes, liposomes coated with DNA, tubular structures, and (aggregated) multilamellar structures, where DNA is sandwiched between lipid bilayers (Gustafsson et al., 1995; Lasic, 1997; Lasic et al., 1997; Huebner et al., 1999; Xu et al., 1999). This conveys partial protection of DNA against degradation. The formation of these structures has been attributed to adhesion-mediated membrane rupture and fusion of liposomes (Huebner et al., 1999).

Received for publication 13 October 2000 and in final form 10 February 2001.

Address reprint requests to Dr. Norbert Maurer, Department of Biochemistry and Molecular Biology, The University of British Columbia, 2146 Health Sciences Mall, Vancouver B.C., Canada V6T 1Z3. Tel.: 604-822-4955; Fax: 604-822-4843; E-mail: nmaurer@interchange.ubc.ca.

0006-3495/01/05/2310/17 $2.00

The major focus of this study is the effect of ethanol and poly(ethylene) glycol (PEG) coatings on the interaction of cationic liposomes with antisense oligonucleotides. Previous work on antisense encapsulation has shown that addition of lipids dissolved in ethanol to an aqueous buffer solution containing antisense oligonucleotide resulted in the formation of small multilamellar liposomes trapping oligonucleotide between the lipid bilayers (Semple et al., 2001). Two possible mechanisms are that the lipids form bilayer structures on hydration that subsequently interact with the oligonucleotides to form multilamellar systems or that oligonucleotide-cationic lipid aggregates act as precursors to the small multilamellar liposomes observed. This paper is aimed at understanding the mechanism behind the formation of these unique structures and is particularly focused on the role of ethanol.

It is shown that in the presence of ethanol small multilamellar liposomes with concentric bilayer shells are formed from large unilamellar vesicles (LUVs) following binding of oligonucleotides. This allows efficient trapping of antisense oligonucleotides between the lamellae of these structures. The ethanol concentrations required for this to happen are very close to the region of breakdown of liposomal structure. At these ethanol concentrations liposomes are morphologically intact; however, the lipid membrane is highly destabilized. Leakage of entrapped solutes is rapid, and lipids can flip-flop across the membrane and exchange easily between liposomes. Furthermore, in the presence of ethanol the interaction of the negatively charged polyelectrolyte with the cationic liposomes leads to domain formation resulting in 1-O-(2′-(ω-methoxypolyethylene-glycol)-succinoyl) (PEG-ceramide (Cer))-depleted regions and regions enriched in antisense oligonucleotide. These are suggested to be the regions were contact is established. The subsequent structural rearrangements are a consequence of this adhesion.

MATERIALS AND METHODS

Materials

The phosphorothioate antisense oligodeoxynucleotides and plasmid DNA (pCMV-luc, 5650 bp) used in this study were generously provided by Inex Pharmaceuticals (Burnaby, Canada). The mRNA targets and sequences of the oligonucleotides are as follows: human c-myc (16-mer), 5′-TAACGTTGAGGGGCAT-3′; human c-myc (15-mer, FITC-labeled), 5′-AACGTTGAGGGGCAT-3′; human ICAM-1, 5′-GCCCAAGCTGGCATCCGTCA-3′; and human EGFR, 5′-CCGTGGTCATGCTCC-3′. 1,2-Distearoyl-*sn*-glycero-3-phosphocholine (DSPC) was purchased from Northern Lipids (Vancouver, Canada), and 1,2-dioleoyl-3-dimethylammoniumpropane (DODAP), 1,2-dioleoyl-sn-glycero-3-phosphoserine-*N*-(7-nitro-2–1,3-benzoxadiazol-4-yl) (NBD-PS), 1,2-dioleoyl-*sn*-glycero-3-phosphoethanolamine (DOPE), 1,2-dioleoyl-*sn*-glycero-3-phosphoethanolamine-*N*-(lissamine rhodamine b sulfonyl) (LRh-PE), and 1,2-dioleoyl-*sn*-glycero-3-phosphoethanolamine-*N*-(7-nitro-2–1,3-benzoxadiazol-4-yl) (NBD-PE) from Avanti Polar Lipids (Alabaster, AL). 1-Hexadecanoyl-2-(1-pyrenedecanoyl)-*sn*-glycero-3-phosphocholine (Py-HPC) and the oligonucleotide-binding dye OliGreen were obtained from Molecular Probes (Eugene, OR). 1-O-(2′-(ω-methoxypolyethylene-glycol)succinoyl)-2-*N*-myristoylsphingosine (PEG-CerC_{14}), radioactively labeled [^{3}H]-PEG-CerC_{14}, and 1-O-(2′-(ω-methoxypolyethylene-glycol)succinoyl)-2-*N*-dodecanoylsphingosine (PEG-CerC_{20}) were provided by Inex Pharmaceuticals. The average molecular weight (MW) of the PEG was 2000. Cholesterol (chol), *n*-octyl β-D-glucopyranoside (OGP), Triton X-100, calcein, FITC-dextran (MW 19,500), dichlorodimethylsilane, sodium hydrosulfite (dithionite), DEAE Sepharose CL6B and Sepharose CL4B were obtained from Sigma (Oakville, Canada). All materials for transmission electron microscopy, including osmium tetroxide, lead citrate, maleic acid, sodium cacodylate, and the embedding resin Embed 812 were purchased from Electron Microscopy Sciences (Fort Washington, PA), and low-melting-point agarose was from Life Technologies (Burlington, Canada). Spectra/Por dialysis tubing (12,000–14,000 molecular weight cut-off) was from Spectrum Medical Instruments (Rancho Dominguez, CA). All other reagents used in this study were of analytical grade.

Liposome preparation

The entrapment of oligonucleotides in preformed liposomes relies on the presence of high concentrations of ethanol. Large unilamellar liposomes in ethanol/buffer solutions were either prepared by addition of ethanol to extruded liposomes or by addition of lipids dissolved in ethanol to an aqueous buffer solution and subsequent extrusion. Both methods give the same entrapment results and are described in greater detail here. 1) After hydration of a lipid film in pH 4 citrate buffer and five freeze/thaw cycles, LUVs were generated by extrusion through two stacked 100-nm filters (10 passes). In the case of DSPC/chol-containing liposomes the extrusion was performed at 60°C. Ethanol was subsequently slowly added under rapid mixing. Typical liposome sizes determined after removal of ethanol by dynamic light scattering were 90 ± 20 nm for the DSPC/chol/PEG-CerC_{14}/DODAP system (20:45:10:25 mol %). Slow addition of ethanol and rapid mixing are important as liposomes become unstable and coalesce into large lipid structures as soon as the ethanol concentration exceeds a certain upper limit. The latter depends on the lipid composition. For example, an initially translucent DSPC/chol/PEG-CerC_{14}/DODAP liposome dispersion becomes milky white if the ethanol concentration exceeds 50% (v/v). 2) LUVs were prepared by slow addition of the lipids dissolved in ethanol (0.4 ml) to citrate buffer at pH 4 (0.6 ml) followed by extrusion through two stacked 100-nm filters (two passes) at room temperature. Dynamic light-scattering measurements performed in ethanol and after removal of ethanol by dialysis show no significant differences in size, which is typically 75 ± 18 nm. The extrusion step can be omitted if ethanol is added very slowly under vigorous mixing to avoid high local concentrations of ethanol.

Entrapment procedure

The oligonucleotide solution was slowly added under vortexing to the ethanolic liposome dispersion, which typically contained 10 mg/ml lipid. It was subsequently incubated at the appropriate temperature for 1 h, dialyzed for 2 h against a 1000-fold volume excess of citrate buffer to remove most of the ethanol and twice against a 1000-fold volume excess of Hepes-buffered saline (HBS: 20 mM HEPES/145 mM NaCl, pH 7.5). These dialysis steps ensure complete removal of ethanol (<0.01% as determined with the alcohol dehydrogenase assay kit from Sigma). At pH 7.5, DODAP becomes charge-neutral, and oligonucleotides bound to the external membrane surface are released from their association with the cationic lipid. Unencapsulated oligonucleotides were subsequently removed by anion exchange chromatography on DEAE-Sepharose CL-6B columns equilibrated in HBS pH 7.5. If not otherwise mentioned, DSPC/chol/PEG-CerC_{14}/DODAP liposomes (20:45:10:25 mol %), anti-c-myc, 40% (v/v) ethanol, 10 mg/ml (13 μmol/ml) of total lipid, 300 mM citrate buffer, and incubation at 40°C were used. Lipid integrity was analyzed by HPLC on a Beckman Gold 128 apparatus equipped with an evaporative light-scattering

detector (SEDEX-55) and a 2-mm × 150-mm, 5-μm Ultrasphere cyanopropyl column (Beckman Instruments, Fullerton, CA) as described in Semple et al. (2001). After incubation at 60°C for 2 h in pH 4 citrate buffer, >98% of all lipid components present in the formulation remained intact. No lipid degradation was detectable at room temperature (25°C) under otherwise the same conditions.

Determination of trapping efficiencies

Trapping efficiencies were determined after removal of external oligonucleotides by anion exchange chromatography. Oligonucleotide concentrations were determined by UV spectroscopy on a Shimadzu UV160U spectrophotometer. The absorbance at 260 nm was measured after solubilization of the samples in chloroform/methanol at a volume ratio of 1:2.1:1 chloroform/methanol/aqueous phase (sample/HBS). If the solution was not completely clear after mixing, an additional 50–100 μl of methanol was added. Alternatively, absorbance was read after solubilization of the samples in 100 mM octylglucoside. The antisense concentrations were calculated according to c (μg/μl) = A_{260}× 1 OD_{260} unit (μg/ml) × dilution factor (ml/μl), where the dilution factor is given by the total assay volume (ml) divided by the sample volume (μl). OD_{260} units were calculated from pairwise extinction coefficients for individual deoxynucleotides, which take into account nearest-neighbor interactions. One OD corresponds to 30.97 μg/ml anti-c-myc, 33.37 μg/ml anti-ICAM-1, and 34 μg/ml anti-EGFR. Lipid concentrations were determined by the inorganic phosphorus assay after separation of the lipids from the oligonucleotides by a Bligh and Dyer extraction (Bligh and Dyer, 1959). Briefly, to 250 μl of aqueous phase (sample/HBS), 525 μl of methanol and 250 μl of chloroform were added to form a clear single phase (aqueous phase/methanol/chloroform 1:2.1:1 vol). If the solution was not clear, a small amount of methanol was added. Subsequently, 250 μl of HBS and an equal volume of chloroform were added. The samples were mixed and centrifuged for 5–10 min at 1700 × g. This resulted in a clear two-phase system. The chloroform phase was assayed for phospholipid content according to the method of Fiske and Subbarow (1925). If not otherwise mentioned, trapping efficiencies were expressed as oligonucleotide-to-lipid weight ratios (w/w).

Preparation of giant liposomes

Giant liposomes were made according to Needham and Evans (1988). Briefly, lipids were dissolved in chloroform. A circular Teflon disk was roughened with emery paper and thoroughly cleaned by washing in detergent, tap water, distilled water, and chloroform. The lipid/chloroform solution was applied with a Hamilton syringe to the rough side of a Teflon disc and spread out over the entire surface. The concentration of total lipid was ~10 mg/ml. The disc was put into a beaker, and the last traces of solvent were removed by evacuation for at least 3 h. The rehydration of the lipid film was carried out above the liquid-crystalline acyl chain phase transition temperature. First, the lipid film was prehydrated at 60°C for 30 min to 1 h with water-saturated argon. Final hydration of the lipid was accomplished by addition of prewarmed buffer. The beaker was sealed and incubated in an oven overnight to allow the lipid to hydrate undisturbed.

Dynamic light scattering

Sizes were determined by dynamic light scattering (DLS) using a NICOMP 370 particle sizer (Nicomp Particle Sizing, Santa Barbara, CA). The cumulant fit, a simple form of polydispersity analysis, was used to obtain the average and relative width of size distributions (Koppel, 1972; Ostrowsky, 1993). This two-parameter fit describes the experimental data with good accuracy as goodness-of-fit values ≤1 demonstrate. Throughout the paper, number-averaged sizes were presented. The viscosity of the ethanol/citrate buffer was determined using an Ubelohde-type viscometer (Cannon 50). The viscosity of ethanol/300 mM citrate buffer (40/60, v/v) at 23°C measured relative to water at the same temperature was found to be 2.674×10^{-3} (Pa · s). The zeta potential was determined by electrophoretic light scattering using a Coulter light-scattering instrument (DELSA, Coulter Electronics, Hialeah, FL).

Lipid flip-flop

Lipid flip-flop was determined by chemical reduction of the fluorescent lipid, NBD-PS, to a nonfluorescent compound with sodium dithionite (McIntyre and Sleight, 1991; Lentz et al., 1997). Liposomes were prepared at 20 mM lipid by extrusion in the presence of 1 mol % NBD-PS. Only NBD-PS located in the outer monolayer is accessible to the reducing agent, dithionite, added to the external medium. Its redistribution from the inner monolayer to the outer can be followed after reduction of NBD-PS in the outer membrane leaflet. A 1 M sodium dithionite solution was freshly prepared in 1 M TRIS. NBD-PS in the outer monolayer was reduced by addition of a 100-fold molar excess of sodium dithionite relative to NBD and incubation for 10 min. The completion of the reaction was checked by measuring the dithionite fluorescence at 520 nm before and after reduction exciting at 465 nm. Excess dithionite was subsequently removed by size exclusion chromatography on a Sephadex G50 column. The liposomes were incubated in the presence of 40% ethanol, and aliquots corresponding to a final lipid concentration of 150 μM were removed for measurement at different time points. The residual ethanol concentration of <1.5% (v/v) in these samples had no effect on membrane permeability. Fig. 4 *C* shows that no influx of dithionite into the liposomes occurred over the time course of the assay (dotted line).

Leakage experiments

Ethanol-induced permeabilization of LUVs was measured at different temperatures and as a function of the size (MW) of the entrapped solute. Calcein was used as a low-MW marker for leakage and FITC-dextran (MW 19500) as a high-MW marker. Leakage of calcein entrapped at self-quenching concentrations was followed by monitoring the dequenching of the calcein fluorescence. LUVs were prepared by hydration of a lipid film with an aqueous solution containing 75 mM calcein and 5 mM HEPES adjusted to pH 7.5 by addition of sodium hydroxide, followed by five freeze/thaw cycles and extrusion through two stacked 100-nm filters (10 passes). In the case of DSPC/chol/PEG-CerC_{14}/DODAP, extrusion was performed at 60°C. Unentrapped calcein was exchanged against an iso-osmotic HBS buffer by anion exchange chromatography on a DEAE Sepharose CL6B column. The liposome stock solution was diluted to a lipid concentration of 3 μM in HBS containing varying amounts of ethanol pre-equilibrated at 25°C, 40°C, or 60°C. The fluorescence at 520 nm was measured (excitation wavelength 488 nm, long-pass filter at 430 nm) with a Perkin-Elmer LS50 fluorimeter (Perkin-Elmer, Norwalk, CT) after 5 min of incubation at the corresponding temperature. The value for 100% leakage (maximum dequenching) was obtained by addition of a 10% Triton X-100 solution to a final concentration of 0.05%. Calcein leakage was calculated according to % leakage = $(F_s - F_b)/(F_{Tx} - F_b) \times 100$, where F_s is the fluorescence of the sample, F_b is the background corresponding to calcein-containing liposomes in the absence of ethanol, and F_{Tx} is the Triton X-100 value.

FITC-dextran (MW 19,500) was entrapped in DSPC/chol/PEG-CerC_{14}/DODAP liposomes incorporating 0.5 mol % LRh-PE at a final concentration of 45 mg/ml. Entrapment was performed by addition of the lipids dissolved in ethanol to the FITC-dextran solution in HBS followed by extrusion (two stacked 100-nm filters, two passes) and subsequent removal of ethanol by dialysis. Unentrapped FITC-dextran was removed by size exclusion chromatography on a Sepharose CL4B column (1.5 × 15 cm). The loss of FITC-dextran from liposomes exposed to 40% ethanol was determined after removal of released FITC-dextran by size exclusion

chromatography on a Sepharose CL4B column (1.5 × 15 cm). The FITC/LRh-PE ratio was measured before and after addition of ethanol. FITC and LRh-PE fluorescence were measured at 515 and 590 nm with the excitation wavelength set to 485 and 560 nm, respectively.

Lipid mixing

Ethanol-induced lipid mixing/exchange was followed by the loss of resonance energy transfer, occurring between a donor, NBD-PE, and an acceptor, LRh-PE, which are in close proximity, upon dilution of the probes into an unlabeled target membrane (Struck et al., 1981). LUVs contained 0.75 mol % of both NBD-PE and LRh-PE. Labeled and unlabeled liposomes were prepared in HBS pH 7.5 by extrusion at lipid concentrations of 20 mM. Ethanol was added to labeled and unlabeled liposomes to a final concentration of 40% (v/v). Subsequently, the ethanolic dispersions of labeled and unlabeled liposomes were mixed at a molar lipid ratio of 1:5 and incubated at the appropriate temperatures. Aliquots were withdrawn at given times and added to 2 ml of HBS to give a final lipid concentration of 150 μM. Emission spectra of NBD and LRh were measured in the region from 505 to 650 nm with the excitation wavelength set to 465 nm (430-nm emission long-pass filter). After background subtraction (unlabeled liposomes at 150 μM lipid) the loss of resonance energy transfer was expressed as the increase in NBD/LRh ratio.

Pyrene-HPC assay

Pyrene-HPC forms excited-state dimers at high concentrations, which fluoresce at a different wavelength from the monomers. Excimer formation is a diffusion-controlled process and requires two molecules to come together to form a dimer. Lipid mixing (target membrane) as well as a decrease in the lateral mobility of pyrene-HPC in the membrane can result in a decrease in pyrene excimer fluorescence (Hoekstra, 1990; Duportail and Lianos, 1996). Lateral phase separation usually results in an increase in pyrene excimer fluorescence (Duportail and Lianos, 1996). The rationale of this experiment was to look at the effect of oligonucleotide binding on the liposomal membrane. The pyrene-HPC fluorescence of liposomes entrapping oligonucleotide was compared with empty control liposomes before and after depletion of the transmembrane pH gradient. Increasing the internal pH to 7.5 results in the release of membrane-bound oligonucleotides. Liposomes incorporating pyrene-HPC at a concentration of 7 mol % were prepared by addition of lipids dissolved in ethanol to pH 4 citrate buffer. An aliquot was removed, and oligonucleotide was entrapped as described above. The remaining initial liposomes were treated the same way in all the subsequent steps (see Entrapment procedure above). The pH gradient was dissipated with ammonium acetate adjusted to pH 7.5. Liposomes were diluted into the appropriate buffer, HBS pH 7.5 or 150 mM ammonium acetate pH 7.5, to a final lipid concentration of 2 μM. Pyrene-HPC emission spectra were recorded in the wavelength region from 365 to 550 nm with excitation at 345 nm and an emission cutoff filter at 350 nm. The intensity ratio of monomer fluorescence at 397 nm to dimer fluorescence at 478 nm was plotted for the initial liposomes as well as for the oligonucleotide-containing liposomes before and after depletion of the pH gradient.

^{31}P NMR spectroscopy

^{31}P NMR spectra were obtained with a Bruker MSL200 spectrometer operating at 81.03 MHz. Free induction decays (FIDs) corresponding to 2400 scans were collected by using a 2.8-μs 50° pulse with a 3-s interpulse delay and a spectral width of 20,000 Hz on a 2.0-ml sample in a 10-mm probe. No proton decoupling was employed. An exponential multiplication corresponding to 25 Hz of line broadening was applied to the FIDs before Fourier transformation. The chemical shift was referenced to external 85% phoshoric acid (H_3PO_4). The spin-lattice relaxation times (T_1) of free and encapsulated oligonucleotides at pH 7.5 are essentially the same with T_1^{free} = 1.7 s and T_1^{enc} = 2.1 s. The T_1 values were measured by an inversion-recovery pulse sequence. The interpulse delay of 3 s for 50° pulses allows for complete relaxation of all antisense resonances.

Ultracentrifugation

Liposomes with and without entrapped oligonucleotides were fractionated by ultracentrifugation on a sucrose step gradient consisting of 1%, 2.5%, 10%, and 15% (w/v) sucrose in HBS pH 7.5 with a step volume of 3.5, 3.5, 2.5, and 1.5 ml, respectively. Samples were centrifuged for 2 h at 36,000 rpm (RCF_{max} 22,1000 × g) using a Beckmann L8–70 ultracentrifuge in combination with a SW41Ti rotor. The gradient was either fractionated from the top or individual bands were removed with a syringe after puncturing the tube with a needle.

Cryo-transmission electron microscopy (cryo-TEM)

A drop of sample was applied to a standard electron microscopy grid with a perforated carbon film. Excess liquid was removed by blotting with filter paper, leaving a thin layer of water covering the holes of the carbon film. The grid was rapidly frozen in liquid ethane, resulting in vesicles embedded in a thin film of amorphous ice. Images of the vesicles in ice were obtained under cryogenic conditions at a magnification of ×66,000 and a defocus of −1.5 μm using a Gatan cryo-holder in a Philips CM200 FEG electron microscope.

Freeze-fracture electron microscopy

Samples were cryo-fixed in the presence of 25% glycerol by plunging them into liquid Freon 22 cooled by liquid N_2. The fractured surface was shadowed unidirectionally with platinum (45°) and coated with carbon (90°) employing a Balzers freeze-etching system BAF 400D (Balzers, Liechtenstein). Replicas were analyzed using a JEOL model JEM 1200 EX electron microscope (Soquelec, Montreal, Canada).

Transmission electron microscopy (TEM)

Samples were fixed by the addition of 1 vol of 2% osmium tetroxide to 0.5 vol of vesicles in HBS followed by centrifugation at 17,000 × g and 4°C for 45 min. Osmium tetroxide reacts with lipids, in particular with the double bonds in unsaturated lipids, as well as with nucleic acids and results in a trilaminar appearance of lipid membranes, corresponding to a dark-light-dark pattern (Hyatt, 1981). The resulting pellet was mixed with an equal volume of 3% agarose/PBS, pipetted onto a microscope slide, and allowed to cool to 4°C. The solidified agarose containing the vesicles was cut into 1-mm pieces and transferred to a glass tube for further processing. The blocks were washed three times for 5 min each with 0.05 M maleic acid pH 5.2 before staining in 2% uranyl acetate for 1 h. The tissue pieces were dehydrated through a graded series of alcohols (50–100%), infiltrated with increasing ratios of epoxy resin (EMbed 812):propylene oxide and embedded in 100% EMbed 812 at 60°C for 24 h. Ultrathin sections were stained with 2% lead citrate and examined using a Zeiss EM 10C transmission electron microscope (Oberkochen, Germany).

Phase contrast and fluorescence microscopy

Phase contrast and fluorescence microscopy were performed on a Zeiss Axiovert 100 microscope using a Plan Apochromat 63×/1.4 NA oil immersion objective in combination with a 1.6× optovar lens and an XF100 filter set from Omega Optical (Brattleboro, VT) with the following optical

specifications: excitation 475 ± 20/dichroic 500/emission 535 ± 22.5. Images were recorded on Kodak Ektachrome P1600 color reversal film at 1600 ISO with a Zeiss MC80 DX microscope camera. Slides and coverglasses were siliconized with dichlorodimethylsilane to neutralize the otherwise negatively charged glass surface.

RESULTS

Choice of lipid components

LUVs composed of DSPC/Chol/PEG-CerC_{14}/DODAP were used in most parts of this study to maintain consistency and comparability with a previous study (Semple et al., 2001). However, it will be shown that other zwitterionic lipids, including DOPE alone or in combination with cholesterol, can be substituted for DSPC/Chol. DODAP was chosen as the cationic lipid because it has a protonable amino group. Its apparent pK_a can be adjusted to values much lower than its intrinsic pK_a, which is estimated to be between 6.6 and 7, by increasing the ionic strength of the solution (which in turn causes a decrease of the proton concentration at the interface and therefore a decrease of ionized DODAP) (Gennis, 1989; Tocanne and Teissie, 1990; Bailey and Cullis, 1994). Therefore, entrapment can be performed at low pH (pH 4) where DODAP is positively charged and nonentrapped oligonucleotides can be dissociated from the cationic lipid by neutralizing the pH and removed by subsequent anion exchange chromatography. Adjusting the pH to 7.5 renders the surface charge of the liposomes neutral. The zeta potential as measured by electrophoretic light scattering was found to be zero at pH 7.5. Binding and dissociation of externally added oligonucleotides can be easily followed by ^{31}P NMR because the ^{31}P NMR signal of phosphorothioate antisense deoxynucleotides is shifted ~56 ppm downfield from the phosphodiester lipid peak (Hirschbein and Fearon, 1997). Oligonucleotides added externally to DODAP/DSPC/Chol/PEG-CerC_{14} LUVs in HBS do not bind at pH 7.5 as demonstrated by the full recovery of the phosphorothioate NMR signal (oligonucleotide-to-lipid weight ratio of 0.1; Fig. 1 *A*). Almost complete loss of the signal at pH 4 is indicative of binding (Fig. 1 *B*). Readjustment of the pH to 7.5 leads to the dissociation of the oligonucleotides and to recovery of the NMR signal (Fig. 1 *C*). Loss of the NMR signal was also observed following oligonucleotide binding in 300 mM citrate buffer at pH 4 (data not shown).

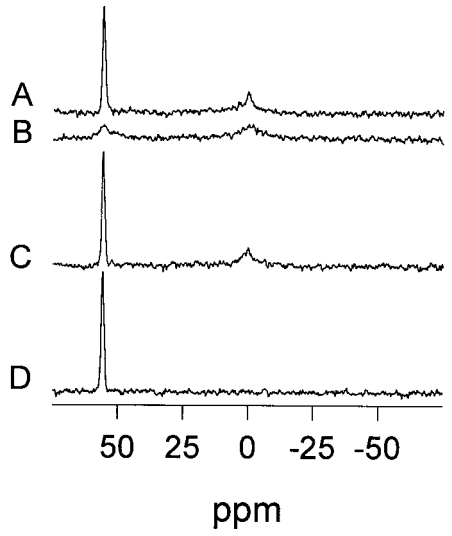

FIGURE 1 Binding and dissociation of oligonucleotide to/from DSPC/Chol/PEG-CerC_{14}/DODAP (20:45:10:25 mol %) liposomes was followed by ^{31}P NMR spectroscopy at different pH values. One milligram of c-myc was added to DSPC/Chol/PEG-CerC_{14}/DODAP liposomes (10 mg/ml lipid) in HBS at pH 7.5 (*A*), after adjustment of the pH to 4 with HCl (*B*), and following readjustment of the pH from 4 to 7.5 (*C*). (*D*) The spectrum of free c-myc at 1 mg/ml. The almost complete loss of the signal at pH 4 is indicative for oligonucleotide binding. No binding is obvious at pH 7.5. The full signal is recovered.

The interaction of cationic liposomes with oligonucleotides in ethanol leads to the formation of multilamellar liposomes, which trap oligonucleotides between the bilayers

The effect of ethanol on the interaction of cationic liposomes with oligonucleotides was studied through the following experiments. Increasing amounts of ethanol were added to 100-nm DSPC/Chol/DODAP liposomes prepared by extrusion. All samples became milky white immediately upon oligonucleotide addition (oligonucleotide-to-lipid ratio 0.3 mg/mg), indicating formation of large lipid structures. Following incubation at pH 4, ethanol was removed, and the pH was adjusted to 7.5 by dialysis against HBS (see Materials and Methods). Table 1 lists encapsulation efficiencies determined after removal of external oligonucleotides by anion exchange chromatography. Due to the large and heterogeneous size of these systems, 30–40% lipid was retained on top of the anion exchange column. Despite lipid loss, the trend is clear. More antisense oligonucleotide becomes entrapped as the ethanol concentration is increased. This is reflected by a progressive reorganization of the LUVs into large multilamellar liposomes (data not presented here; however, see the TEM micrograph shown in Fig. 6 *C* for a sample prepared in 30% ethanol). The size

TABLE 1 Entrapment of antisense oligonucleotide in the absence of PEG-Cer

% EtOH [v/v]	% Encapsulation
0	4.5 ± 0.5
20	20.5 ± 1.5
30	32.5 ± 2.5

Encapsulation efficiencies are listed as a function of ethanol concentration for DSPC/chol/DODAP (30:45:25 mol %) LUVs. The initial oligonucleotide-to-lipid ratio was 0.034 mol/mol (0.3 mg/mg). The LUVs used for these experiments were 99 ± 22 nm in size. The encapsulation values are given as mean ± SD.

and heterogeneity in size in these systems is large. At ethanol concentrations of 40% and higher the initial liposomes became unstable and fused to form a milky white dispersion.

Incorporation of PEG-Cer allows control of liposome size

From the previous results it is apparent that ethanol makes the lipid membrane susceptible to structural rearrangements that are triggered by the addition of the oligonucleotide and ultimately lead to the formation of multilamellar liposomes and oligonucleotide entrapment. However, the size of the liposomes formed cannot be readily controlled. It was found that inclusion of 2.5–10 mol % of PEG-Cer into the liposomes allows the final size of the antisense-containing liposomes to be regulated. Liposomes were stable at higher ethanol concentrations in the presence of PEG-Cer than in its absence. The dispersions remained optically translucent in 40% (v/v) ethanol, although a slight increase in turbidity was noted for the sample containing 2.5 mol % PEG-Cer. The increased stability is also reflected in the higher amounts of ethanol required for entrapment to occur (Table 2; Fig. 2 *A*). Fig. 2 *A* depicts encapsulation efficiencies as a function of ethanol concentration for liposomes containing 10 mol % PEG-Cer. Maximum entrapment was reached at 40% ethanol, and ethanol concentrations in excess of 25% (v/v) (>4.3 M) were required for entrapment to occur. No entrapment was found in the absence of ethanol. Table 2 lists trapping efficiencies and average sizes as a function of PEG-Cer content (2.5–10 mol %) at the minimum and maximum ethanol concentrations determined from Fig. 2 *A*. The amount of ethanol required for entrapment to occur depends on the PEG-Cer content of the liposomes. Liposomes containing 2.5 mol % PEG-Cer entrapped ~15% of the oligonucleotides at 25% ethanol and 45% in the presence of 40% ethanol. In contrast, at 10 mol % PEG-Cer, entrapment was virtually abolished in the presence of 25% ethanol (≤5%) and was 60% in 40% ethanol. In all cases, the initial oligonucleotide-to-lipid ratio was 0.037 (mol/mol). Entrapment levels increased from 45% to almost 60% in 40% ethanol when the PEG-Cer content was increased from 2.5 to 10 mol %. Liposome size and polydispersity decreased from 131 ± 40 nm to 100 ± 26 nm. All subsequent studies were performed using preformed liposomes containing 10 mol % PEG-Cer.

TABLE 2 Effect of PEG-Cer on entrapment

$PEG\text{-}CerC_{14}$ (mol %)	% Encapsulation	Average size and polydispersity (nm)
25% ethanol		
2.5	14 ± 1.5	125 ± 35 (108 ± 26)
10	5 ± 1	92 ± 18 (93 ± 18)
40% ethanol		
2.5	45.5 ± 3	131 ± 40 (108 ± 26)
5	51 ± 1.5	126 ± 36 (107 ± 22)
10	56.5 ± 2	100 ± 26 (93 ± 18)

Encapsulation efficiencies and number-averaged sizes determined by dynamic light scattering are listed as a function of $PEG\text{-}CerC_{14}$ content at two different ethanol concentrations. The sizes of the initial extruded liposomes are given in parentheses. The decrease in PEG-Cer content was offset by an increase in the amount of DSPC (DSPC/chol/$PEG\text{-}CerC_{14}$/DODAP ($20 + x$:45:10 − x:25 mol %)). The initial oligonucleotide-to-lipid ratio was 0.037 mol/mol. The encapsulation values are given as mean ± SD.

Effect of ethanol on liposome stability

The perturbing effect of ethanol on lipid membranes has been mainly studied at low ethanol concentrations (<15% v/v) in relation to changes in lipid hydration, acyl chain order, membrane permeability to small ions, and induction of chain interdigitation in DPPC systems (Slater and Huang, 1988; Barchfeld and Deamer, 1988; Schwichtenhovel et al., 1992; Slater et al., 1993; Barry and Gawrisch, 1995; Vierl et al., 1994; Lobbecke and Cevc, 1995; Komatsu and Okada, 1996; Holte and Gawrisch, 1997). It is logical to ask whether liposomes are still intact at the high ethanol concentrations required for entrapment. Fig. 2 *A* depicts the release of calcein entrapped at self-quenching concentrations in DSPC/Chol/$PEG\text{-}CerC_{14}$/DODAP liposomes as a function of ethanol concentration (closed circles) together with the encapsulation efficiencies obtained using liposomes of the same lipid composition (open circles). Both the encapsulation as well as the leakage experiments were performed at 40°C. Leakage of calcein, a small molecule with a MW of 623, starts at ≥30% ethanol and reaches a maximum around 40% ethanol. The oligonucleotide entrapment shows a similar ethanol dependence, indicating that the entrapment is highly correlated with the destabilization of the liposomal membrane permeability barrier. In contrast to calcein, the release of FITC-dextran (MW 19,500) was less than 10% in 40% ethanol. This shows that the loss of the permeability barrier is MW dependent, as has also been reported for detergents such as octylglucoside and sodium cholate (Almog et al., 1990; Schubert et al., 1991). The liposomes maintained their morphology in the presence of 40% ethanol. Phase contrast microscopy of giant liposomes in 40% ethanol also revealed intact liposomal structures (see Fig. 8 *A*, *left side*).

Lipids are also able to exchange rapidly between liposomes and between the inner and outer monolayers of the lipid bilayers comprising the liposomes. As shown in Fig. 2 *B* (open symbols), lipid mixing as detected by the NBD-PE/LRh-PE fluorescence resonance energy transfer (FRET) assay is effectively immediate in 40% ethanol. No increase in vesicle size was observed, indicating the lipid mixing is arising from rapid lipid exchange between liposomes rather than liposome fusion. The results shown in Fig. 2, *B* (closed symbols) and *C*, also demonstrate that lipids are able to rapidly translocate (flip-flop) from one side of the liposomal

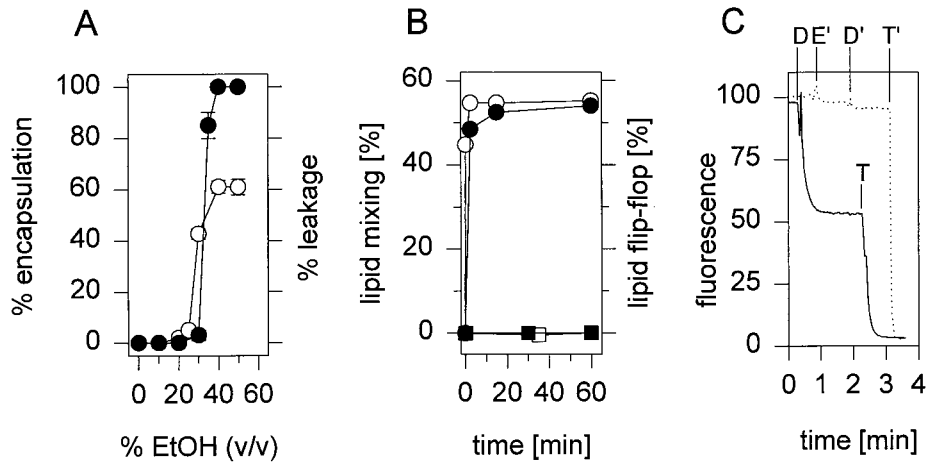

FIGURE 2 (*A*) Encapsulation as a function of ethanol concentration and correlation between ethanol-induced membrane destabilization and entrapment. The release of calcein entrapped at self-quenching concentrations in DSPC/Chol/PEG-CerC_{14}/DODAP (20:45:10:25 mol %) liposomes is shown as a function of ethanol concentration (●) together with the encapsulation efficiencies obtained using liposomes of the same lipid composition (○). Entrapments were performed at an initial oligonucleotide-to-lipid ratio of 0.24 mg/mg. (*B*) Lipid exchange (○ and □) and lipid flip-flop (● and ■) at 40°C in the presence and absence of ethanol. Lipid exchange as well as lipid flip-flop are rapid in 40% ethanol (○ and ●) and do not occur to significant levels in its absence (□ and ■). Lipid mixing was followed by the NBD-PE/LRh-PE FRET assay according to Struck et al. (1981) and lipid flip-flop by reduction of NBD-PS redistributing to the outer lipid monolayer. (*C*) Time course of the NBD-PS reduction. The full line represents the first time point shown in *B* (●) after addition of dithionite (denoted by D) and Triton X-100 (denoted by T). The dotted line represents the initial sample, where NBD-PS located in the outer monolayer had been reduced, after addition of ethanol to 1.5% (v/v) (denoted by E′), dithionite (denoted by D′) and Triton X-100 (denoted by T′).

lipid bilayer to the other, as shown by the loss in fluorescence of NBD-PS located in the outer lipid monolayer upon chemical reduction with sodium dithionite.

Entrapment is preceded by an aggregation step

The increase in turbidity upon encapsulation indicates that entrapment is preceded by an initial aggregation step (formation of microaggregates). The aggregation step and the entrapment can be decoupled at low temperatures. Samples become turbid upon or shortly after addition of oligonucleotide, and the turbidity increases over time (results not shown). In the absence of ethanol, there is only a slight increase in turbidity following which light transmission remains constant. In contrast to samples prepared at 40°C, samples incubated at 4°C become translucent again when ethanol is removed and liposomes do not entrap oligonucleotide. Entrapment efficiencies are plotted as a function of temperature in Fig. 3 together with calcein leakage data. Leakage data are presented as the ethanol concentrations required to induce 50% calcein release. Again, there is a qualitative correlation between the destabilization of the liposomal membrane and the entrapment efficiency.

Entrapment and location of entrapped oligonucleotides

^{31}P NMR can be used to assay for oligonucleotide entrapment. Fig. 4 shows ^{31}P NMR spectra of anti-c-myc in solution (Fig. 4 *A*) and entrapped in DODAP/DSPC/Chol/PEG-CerC_{14} liposomes (Fig. 4 *B*). Initially, the liposomes exhibited a transmembrane pH gradient, where the internal pH is 4 and the external pH is 7.5. Under these conditions the entrapped oligonucleotides are tightly associated with the positively charged liposomal membrane. This immobi-

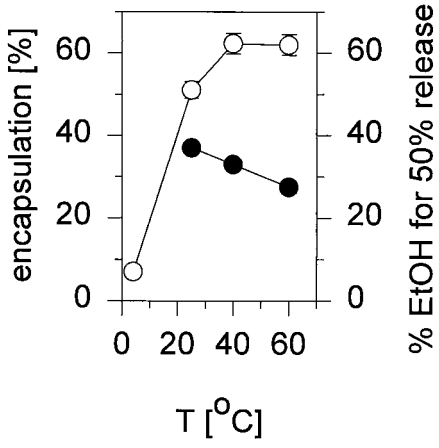

FIGURE 3 Effect of temperature on encapsulation at a fixed ethanol concentration (40%, v/v) (○) and on membrane permeability (●). Oligonucleotides were added to liposomes in ethanol/citrate buffer followed by incubation and removal of ethanol at the indicated temperatures. The initial oligonucleotide-to-lipid ratio was 0.23 mg/mg. The loss of the permeability barrier was followed by the release of calcein entrapped at self-quenching concentrations (75 mM) in DSPC/Chol/PEG-CerC_{14}/DODAP (20:45:10:25 mol %) liposomes. Leakage data are presented as the ethanol concentration required to induce 50% calcein release.

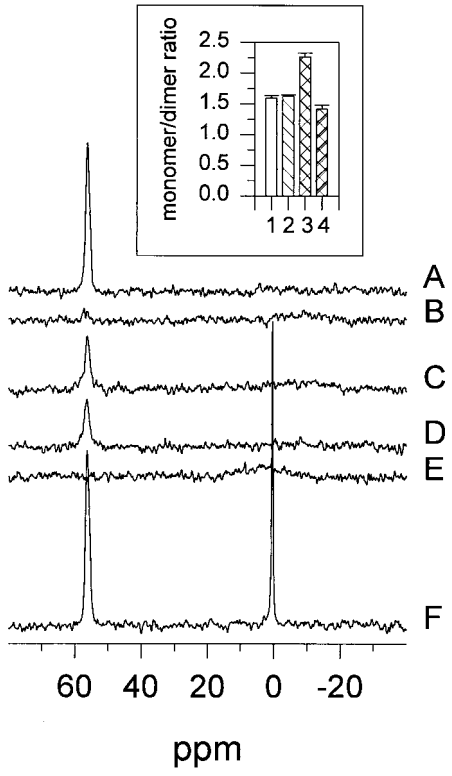

FIGURE 4 Location of entrapped antisense oligonucleotides as determined by ^{31}P NMR. The ^{31}P NMR spectra are presented in the following order: (*A*) 0.5 mg/ml free anti-c-myc; (*B*) liposomally entrapped anti-c-myc at 0.54 mg/ml; (*C*) pH gradient dissipated by incubation in 150 mM ammonium acetate; (*D*) external addition of 5 mM $MnSO_4$; (*E*) detergent (200 mM OGP) added to *D*; (*F*) OGP added to the initial liposomes (*B*) in the absence of Mn^{2+}. The inset shows the effect of oligonucleotide binding and release on lateral lipid mobility followed by changes in excimer fluorescence of pyrene-HPC. Pyrene-HPC was incorporated at a concentration of 7 mol % into the liposomal membrane. The monomer-to-dimer ratio ($F_{397\ nm}/F_{478\ nm}$) is plotted for liposomes, which do not entrap oligonucleotides (LUV in HBS (*1*) and ammonium acetate (*2*)) and liposomes, which do (liposomes entrapping oligonucleotide at an oligonucleotide-to-lipid ratio of 0.13 mg/mg in HBS (*3*) and in ammonium acetate (*4*)). The latter corresponds to the situations *B* and *C* of the NMR data, where oligonucleotide is initially bound (pH gradient) and then dissociated from the membrane by depletion of the pH gradient in 150 mM ammonium acetate pH 7.5.

lization results in the disappearance (broadening out) of the NMR signal (Fig. 4 *B*). Upon dissipation of the pH gradient by addition of ammonium acetate and adjustment of the external pH to 7.5 DODAP is deprotonated and the oligonucleotides dissociate from the liposomal membrane. This is demonstrated by the recovery of the NMR signal in Fig. 4 *C*. However, the recovery is incomplete, ~50% of the initial signal, in contrast to the full signal recovery observed upon external addition of oligonucleotide to cationic DODAP/DSPC/Chol/PEG-CerC_{14} LUVs followed by adjustment of the pH to 7.5 (Fig. 1). The signal attenuation is not due to NMR resonance saturation (see Materials and Methods). It may be attributed to two possibilities: 1) either the amount of encapsulated antisense exceeds its solubility so that a portion of it precipitates or 2) the mobility of the antisense molecules is spatially constrained, e.g., by immobilization between two closely apposing bilayers (see Fig. 6 *A*). To confirm that the oligonucleotides were encapsulated and localized in the aqueous interior of the liposomes, 5 mM $MnSO_4$ was added to the external solution (Fig. 4 *D*). Mn^{2+} is a membrane-impermeable paramagnetic line-broadening agent and will quench the signals of all accessible phosphate groups, phospholipids as well as oligonucleotides. However, the oligonucleotide signal remained unaffected and disappeared only upon solubilization of the liposomes with OGP (Fig. 4 *E*). The whole oligonucleotide signal is recovered when the initial liposomes (Fig. 4 *B*) are solubilized with OGP in the absence of Mn^{2+} (Fig. 4 *F*). These data clearly demonstrate that the oligonucleotide is entrapped in the liposomes and not simply associated with the external membrane. It should also be noted that entrapped oligonucleotides were not accessible to the oligonucleotide-binding dye OliGreen.

The NMR studies describe the interaction between oligonucleotides and liposomes as seen from the perspective of the oligonucleotides. Changes in lipid dynamics and membrane organization can be probed with pyrene-labeled lipids (Duportail and Lianos, 1996). Pyrene-labeled lipids form excited-state dimers at high concentrations, which fluoresce at a different wavelength than the monomers. Excimer formation is a diffusion-controlled process and requires two molecules to come together to form a dimer. The binding of the oligonucleotides results in a dramatic reduction of the lateral mobility of all lipid species relative to control liposomes, which do not contain oligonucleotides (Fig. 4, *inset*, *1-4*). The membrane is laterally compressed. This follows from the observed decrease in excimer fluorescence of pyrene-HPC (*3*). The depletion of the transmembrane pH gradient results in an increase of the excimer fluorescence and restoration of lipid mobility (*4*). Control liposomes in the absence of oligonucleotide are shown in Fig. 4, *inset*, *1* and *2*.

Liposome size and entrapment efficiency

Both the size of the liposomes entrapping antisense as well as the entrapment efficiency depend on the initial oligonucleotide-to-lipid ratio. Fig. 5 shows that oligonucleotides can be efficiently entrapped at high oligonucleotide-to-lipid ratios. The entrapment efficiency is plotted as a function of the initial oligonucleotide-to-lipid ratio. The binding level at maximum entrapment is 0.16 mg of oligonucleotide per mg of lipid (0.023 mol/mol, negative-to-positive charge ratio = 1.5). This corresponds to ~2200 oligonucleotide molecules per 100-nm liposome and demonstrates the high efficiency of this entrapment procedure. Entrapment efficiencies are

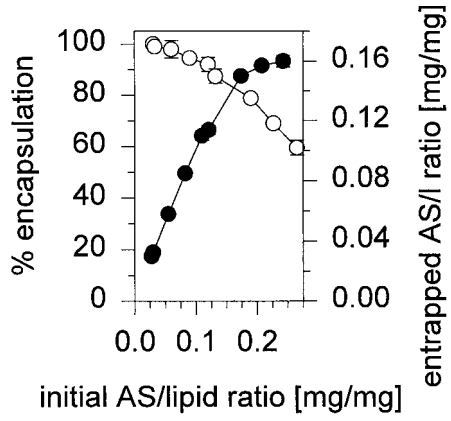

FIGURE 5 Plot of the entrapment efficiency expressed as the entrapped oligonucleotide-to-lipid ratio (●) and percent entrapment (○) as a function of the initial oligonucleotide-to-lipid ratio. The ratios are given in w/w.

~3 orders of magnitude higher than obtained by passive encapsulation based on the trapped volume.

Upon increasing the oligonucleotide-to-lipid ratio, the size as well as the polydispersity of the samples increase slightly from 70 ± 10 nm for liposomes alone to 110 ± 30 for an initial oligonucleotide-to-lipid weight ratio of 0.2 mg/mg. Freeze-fracture electron microscopy showed an increase in the number of larger liposomes with increasing initial oligonucleotide-to-lipid ratios. As an aside, it should be noted that the initially translucent liposome dispersion becomes increasingly turbid as the oligonucleotide-to-lipid ratio is increased.

Morphology

Freeze-fracture images are consistent with a liposomal system; however, internal structure is not revealed (data not shown). Structural details were visualized by cryo-TEM. Fig. 6 *A* is a cryo-TEM image of a sample with an entrapped oligonucleotide-to-lipid ratio of 0.13 mg/mg. It shows that unilamellar liposomes co-exist with bi- and multilamellar liposomes. The membranes of the latter are in close contact. The inset of Fig. 6 *A* is an expanded view of a multilamellar liposome and shows two initially separate membranes forced into close apposition by bound oligonucleotides. In some liposomes, the inter-bilayer binding is discontinuous and the outer membrane exhibits bulbs. The number of multilamellar liposomes increases with increasing initial oligonucleotide-to-lipid ratio. The initial liposomes in the absence of antisense oligonucleotide were unilamellar (Fig. 6 *B*). The existence of multilamellar liposomes can only mean that more than one liposome has to participate in their formation and points to an adhesion-mediated mechanism of formation.

PEG-Cer is displaced from the liposomal membrane upon oligonucleotide entrapment

It would be expected that the PEG coating would inhibit formation of the closely apposed membranes observed for the multilamellar structures by TEM. The fate of PEG-Cer was therefore examined by using radioactively labeled PEG-CerC_{14}. Antisense oligonucleotides were encapsulated in liposomes containing trace amounts of [^{3}H]-PEG-CerC_{14} in addition to 10 mol % unlabeled PEG-CerC_{14} and [^{14}C]-cholesterol hexadecylether (CHE) as a cholesterol marker at a [^{3}H]/[^{14}C] ratio of 5.9. This ratio represents an apparent PEG-Cer/chol ratio and will be used in place of the molar PEG-Cer/chol ratio. The initial oligonucleotide-to-lipid weight ratio was 0.29 mg/mg. Entrapment resulted in a final oligonucleotide-to-lipid ratio of 0.16 mg/mg. Free PEG-Cer and PEG micelles were separated from liposomes by ultracentrifugation using a sucrose step gradient (1%, 2.5%, 10%, and 15% (w/v) sucrose in HBS). Empty liposomes band at the interface between 2.5% and 10% sucrose with an apparent PEG-Cer/chol ratio of 5.5. This band accounts for roughly 80% of the total lipid. The oligonucleotide-containing liposomes show a faint band at the same location, which corresponds to less than 9% of total lipid. However, most of the liposomal antisense oligonucleotide migrates down to the 15% sucrose layer or pellets at the bottom. A complete analysis of the liposome-containing fractions of the gradient is presented in Table 3. The results are representative for samples prepared at high oligonucleotide-to-lipid ratios. It can be seen that the PEG-Cer/chol ratios progressively decrease toward the bottom of the gradient. More than 50% of the PEG-Cer is lost from the bottom fraction relative to the initial liposomes (apparent PEG-Cer/chol ratio 5.5). The DSPC/Chol ratio does not change, indicating that the initial lipid composition is maintained.

Further analysis of the fractions of the above gradient show that the oligonucleotide-containing liposomes show large differences in their oligonucleotide content. The oligonucleotide-to-lipid ratios as well as the average size increase from top to bottom (Table 3). Three main populations can be identified as distinct bands (Table 4): first, liposomes entrapping oligonucleotide at low oligonucleotide-to-lipid ratio (0.03–0.05 mg/mg); second, liposomes with an oligonucleotide-to-lipid ratio of 0.14–0.15 mg/mg; and finally, liposomes with very high oligonucleotide-to-lipid ratios (0.29 mg/mg). Their relative proportions depend on the initial oligonucleotide-to-lipid ratio. The population with high oligonucleotide-to-lipid ratio, which is larger in size than the others, decreases in favor of the first two populations with decreasing initial oligonucleotide-to-lipid ratio. This is consistent with the decrease in average size observed with decreasing oligonucleotide-to-lipid ratio (see dynamic light-scattering data presented above). It was attempted to correlate the observed differences in entrapment and size to the morphological heterogeneity seen by cryo-TEM (Fig. 6). Anti-c-myc oligonucleotide was entrapped at high initial oligonucleotide-to-lipid ratio (0.28 mg/mg), and the two

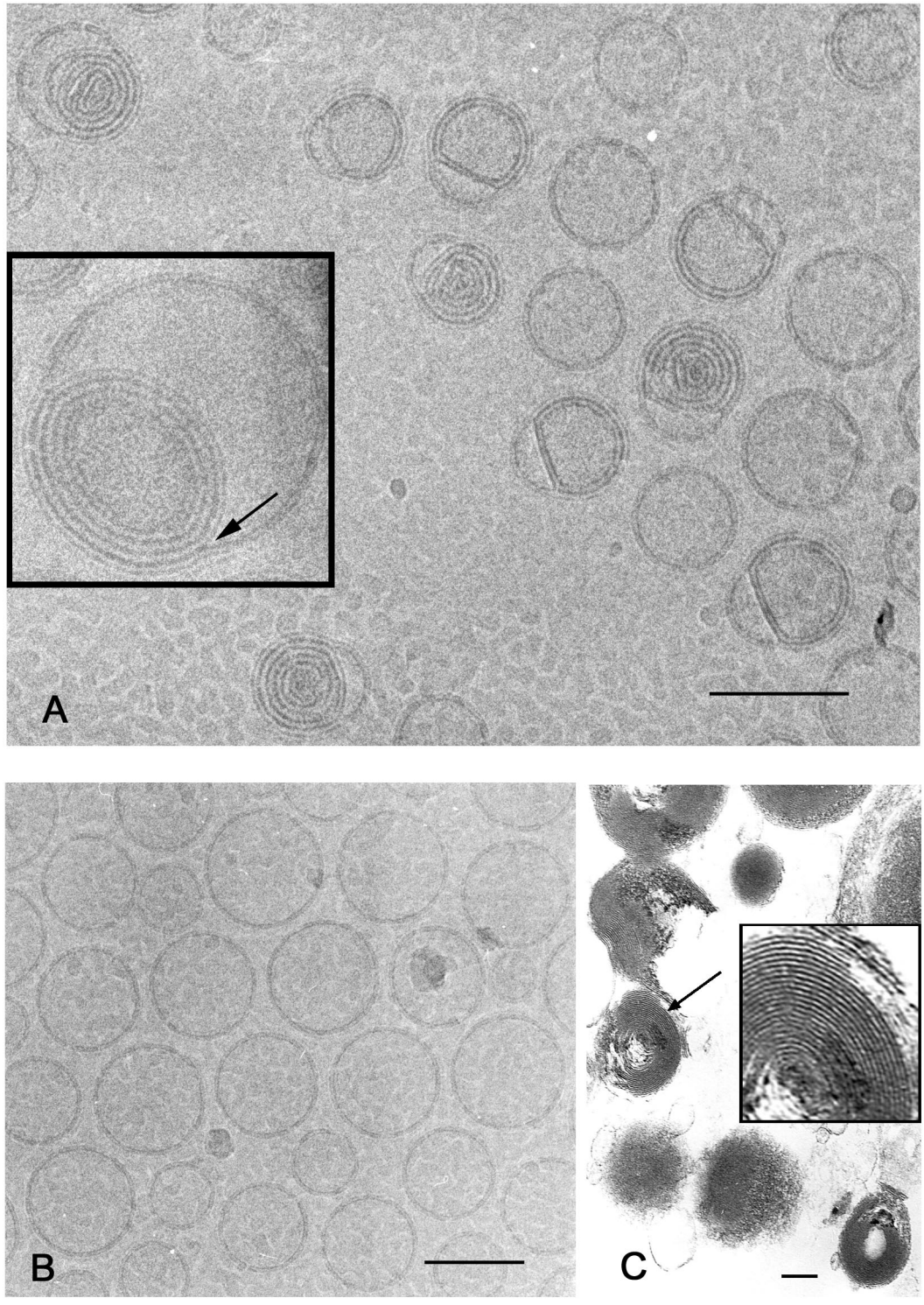

FIGURE 6 (*A*) Cryo-TEM picture of DSPC/Chol/PEG-CerC_{14}/DODAP (20:45:10:25 mol %) liposomes entrapping oligonucleotides. The inset is an expanded view of a multilamellar liposome showing two initially separate membranes forced into close apposition by bound oligonucleotides (indicated by the *arrow*). The entrapped antisense-to-lipid weight ratio was 0.125 mg/mg. Empty liposomes prepared the same way as the oligonucleotide-containing liposomes can be seen in *B*. (*C*) TEM electron micrograph of a sample prepared in 30% ethanol in the absence of PEG-Cer before anion exchange chromatography. The concentric bilayers of multilamellar liposomes can be clearly seen. The inset shows the area indicated by the arrow enlarged by a factor of 3. The entrapment was 32% at an initial oligonucleotide-to-lipid weight ratio of 0.3 mg/mg. Bars, 100 nm.

TABLE 3 Analysis of the lipid composition

Fraction	% PEG-Cer	% Chol	% DSPC	Chol/DSPC (mol/mol)	PEG-Cer/chol ratio (r.u.)	Size (nm)
SBU				2.2	5.9	86 ± 24
1–10	26.8	6.6	ND	ND	ND	ND
11	13.7	9.2	ND	ND	8.6	89 ± 21
12	4.3	3.9	ND	ND	6.4	ND
13	3.6	4.1	ND	ND	5.0	ND
14	8.9	11.4	ND	ND	4.5	83 ± 21
15	27.1	36.6	37.6	2.2	4.2	70 ± 15
16	8.5	12.8	ND	ND	3.8	75 ± 16
17	7.1	15.4	15.5	2.2	2.6	129 ± 39

Antisense oligonucleotides were encapsulated in liposomes containing trace amounts of [^{3}H]-PEG-CerC_{14} in addition to 10 mol % unlabeled PEG-CerC_{14} and [^{14}C]-cholesterol hexadecylether as a cholesterol marker at a [^{3}H]/[^{14}C] ratio of 5.9. The initial oligonucleotide-to-lipid weight ratio was 0.29 mg/mg. Entrapment resulted in a final oligonucleotide-to-lipid weight ratio of 0.156 mg/mg. Free PEG-Cer and PEG-Cer micelles were separated from oligonucleotide-containing liposomes by ultracentrifugation using a sucrose step gradient, and 800 μl of sample containing 4.3 μmol (3.28 mg) of lipid and 0.096 μmol (0.51 mg) of entrapped oligonucleotide were applied to the gradient. The analysis of this gradient is presented above. The recovery of lipids and antisense from the gradient was almost quantitative (>95%). DSPC concentrations were determined by the phosphate assay according to Fiske and Subbarow (1925). The theoretical molar cholesterol-to-DSPC ratio is 2.25 (45/20). SBU, sample before ultracentrifugation; ND, not determined. The [^{3}H]/[^{14}C] ratio is an apparent PEG-Cer/chol ratio and is used instead of the molar PEG-Cer/chol ratio.

main fractions corresponding to fractions 15 and 17 in Table 4 were viewed by cryo-TEM after removal of sucrose by dialysis. The upper fraction consists exclusively of bilamellar liposomes exhibiting bulbs (Fig. 7 *A*) whereas the bottom fraction contained a mixture of bi- and multilamellar liposomes (Fig. 7 *B*).

The addition of oligonucleotides to cationic liposomes in the presence of ethanol can give rise to domain formation

The formation of the multilamellar liposomes seen in Fig. 6 must be preceded by liposome adhesion. However, 10 mol % PEG-Cer completely inhibits adhesion in the absence of ethanol. Two effects could contribute to liposome adhesion in the presence of ethanol: first, the increase in the amount of non-membrane-incorporated PEG-Cer through rapid lipid exchange, and second, formation of small domains depleted in PEG-Cer and enriched in antisense oligonucleotides. The latter possibility was investigated as follows. The effect of oligonucleotide binding was visualized by phase contrast and fluorescence microscopy using giant DSPC/Chol/DODAP/PEG-CerC_{14} liposomes in conjunction with FITC-labeled oligonucleotides. All images represent thin sections of the giant liposomes. Most of these liposomes are multilamellar and display internal structure (Fig. 8 *left side*, *A* (in the absence of ethanol), and *B* (in 40% ethanol)). If ethanol is absent, the giant liposomes disintegrate into irregularly shaped aggregates and smaller liposomes on addition of antisense (Fig. 8 *A*, phase contrast image in the center and fluorescence image on the *right side*). The green FITC fluorescence reveals the location of the oligonucleotides. A completely different picture is presented in the presence of 40% ethanol. The initially round liposomes adopt a pear-shaped form 5–10 min after addition of oligonucleotide with the oligonucleotides located in a semicircle on one side of these structures (Fig. 8 *B*, phase contrast image in the center and fluorescence image on the *right side*). The interior membranes are squeezed out from this horseshoe, which detaches and collapses, particularly upon raising the temperature, into a compact slightly irregular structure that appears completely green in fluorescence. The segregation of the oligonucleotides indicates that ethanol is able to facilitate domain formation.

TABLE 4 Heterogeneity of liposome-encapsulated antisense samples as a function of the entrapped oligonucleotide-to-lipid ratio

	High initial ODN/l ratio			Low initial ODN/l ratio		
Fraction	% Lipid	% ODN	ODN/l	% Lipid	% ODN	ODN/l
SBU	ND	ND	0.156	ND	ND	0.1
11	9.2	1.9	0.030	15.7	6.7	0.036
12	3.9	3.1	0.117	14.8	8.9	0.050
13	4.1	3.9	0.140	3.8	3.4	0.09
14	11.4	10.5	0.140	8.1	11.2	0.14
15	36.6	36.2	0.148	31.5	45.9	0.146
16	12.8	14.4	0.168	9.7	15.4	0.16
17	15.4	30.1	0.29	5.3	8.5	0.162

Oligonucleotide was entrapped at a high (0.156 mg/mg) and at a low (0.1 mg/mg) final oligonucleotide-to-lipid ratio. The samples were fractionated in their component populations by ultracentrifugation on a sucrose gradient. ^{3}H-CHE was used to determine lipid concentrations. The oligonucleotide-to-lipid (ODN/l) ratios are weight ratios (mg/mg). SBU, sample before ultracentrifugation; ND, not determined.

The encapsulation procedure can be applied to other polynucleotides and can employ other lipid compositions

Experiments were conducted to demonstrate that the entrapment is a general feature of the interaction of negatively charged polyelectrolytes with cationic liposomes.

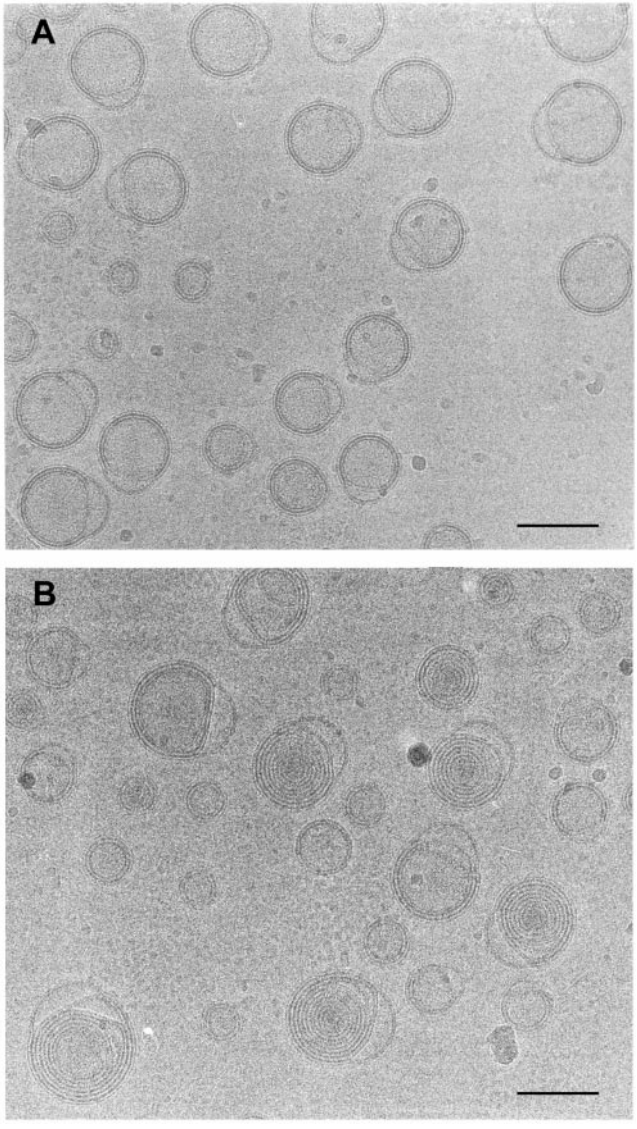

FIGURE 7 Structural heterogeneity of liposomes encapsulating antisense oligonucleotides. A sample prepared at an initial oligonucleotide-to-lipid ratio of 0.28 mg/mg was fractionated in its component liposome populations by ultracentrifugation on a sucrose step gradient. The morphology of the liposomes in the two main fractions was determined by cryo-TEM. The oligonucleotide-to-lipid ratios in these fractions were 0.2 mg/mg (*A*) and 0.32 mg/mg (*B*), respectively. The fraction with the lower oligonucleotide-to-lipid ratio consists exclusively of bilamellar liposomes (*A*). Most of these liposomes exhibit bulbs, and the binding of the bilayers is discontinuous. The fraction with the higher entrapped oligonucleotide-to-lipid ratio consists of a mixture of bi- and multilamellar liposomes (*B*). Bars, 100 nm.

Fig. 9 (*solid bars*) shows that other oligonucleotides than anti-c-myc as well as plasmid-DNA can be efficiently entrapped in DSPC/Chol/DODAP/PEG-CerC_{14} liposomes. The entrapment procedure can also be extended to other lipid compositions including DOPE systems (Fig. 9, *open bars*).

DISCUSSION

The use of membrane-destabilizing agents such as ethanol in conjunction with PEG-lipids offers a new way to control and modulate the interaction between highly charged polymers and cationic liposomes. Ethanol can induce the formation of multilamellar liposomes with concentric bilayer shells from cationic LUVs, thereby trapping oligonucleotides between the lamellae of these multilamellar vesicles (MLVs). The use of a cationic lipid with a protonable headgroup allows dissociation of aggregates and multilamellar structures with nonconcentric bilayer shells such as bilayer stacks and easy removal of unentrapped oligonucleotides. Furthermore, incorporation of PEG-lipids into the liposome membrane allows control of the size of the multilamellar liposomes. In the presence of PEG lipids, small MLVs form, which are not significantly different in their size distribution than the parent LUVs from which they originated. Trapping efficiencies are 3 orders of magnitude higher than achieved by passive encapsulation based on the trapped volume. The following discussion will focus on the formation of these multilamellar liposomes with regard to differences as compared with complexes, the influence of PEG-Cer on liposome size, and the mechanism of formation of these multilamellar liposomes.

Cationic liposome/DNA complexes exhibit a large variety of different structures, including clusters of aggregated liposomes with flat double-bilayer diaphragms in the areas of contact, liposomes coated with DNA, and (aggregated) multilamellar structures, where DNA is sandwiched between lipid bilayers (Gustafsson et al., 1995; Lasic, 1997; Lasic et al., 1997; Huebner et al., 1999; Xu et al., 1999). The latter structures can be flat stacks of bilayers or liposomes, which frequently exhibit nonconcentric bilayer segments on their outer surface. Similar structures have been observed following binding of Ca^{2+} to negatively charged liposomes (Papahadjopoulos et al., 1975; Miller and Dahl, 1982; Rand et al., 1985; Kachar et al., 1986). The structural transformations occurring in these systems were attributed to adhesion-mediated processes such as bilayer rupture and fusion (Rand et al., 1985; Kachar et al., 1986; Huebner et al., 1999). First, liposomes aggregate cross-linked by DNA or Ca^{2+}. Rapid spreading of the contact area deforms the liposomes as they flatten against each other. This places the bilayer under increased tension. If the tension (adhesion energy) is high enough, the stress imposed on the lipid membrane can be relieved either by fusion (increase in area/volume ratio) and/or rupture (volume loss). Most bilayers rupture when the area is increased by ~3% (Evans and Parsegian, 1983). Upon bilayer rupture vesicles collapse, flattening against each other to form multilamellar stacks. Membrane-destabilizing agents such as ethanol can modulate the structural rearrangements occurring upon interaction of cationic liposomes with DNA or oligonucleotides. The multilamellar liposomes observed in the presence

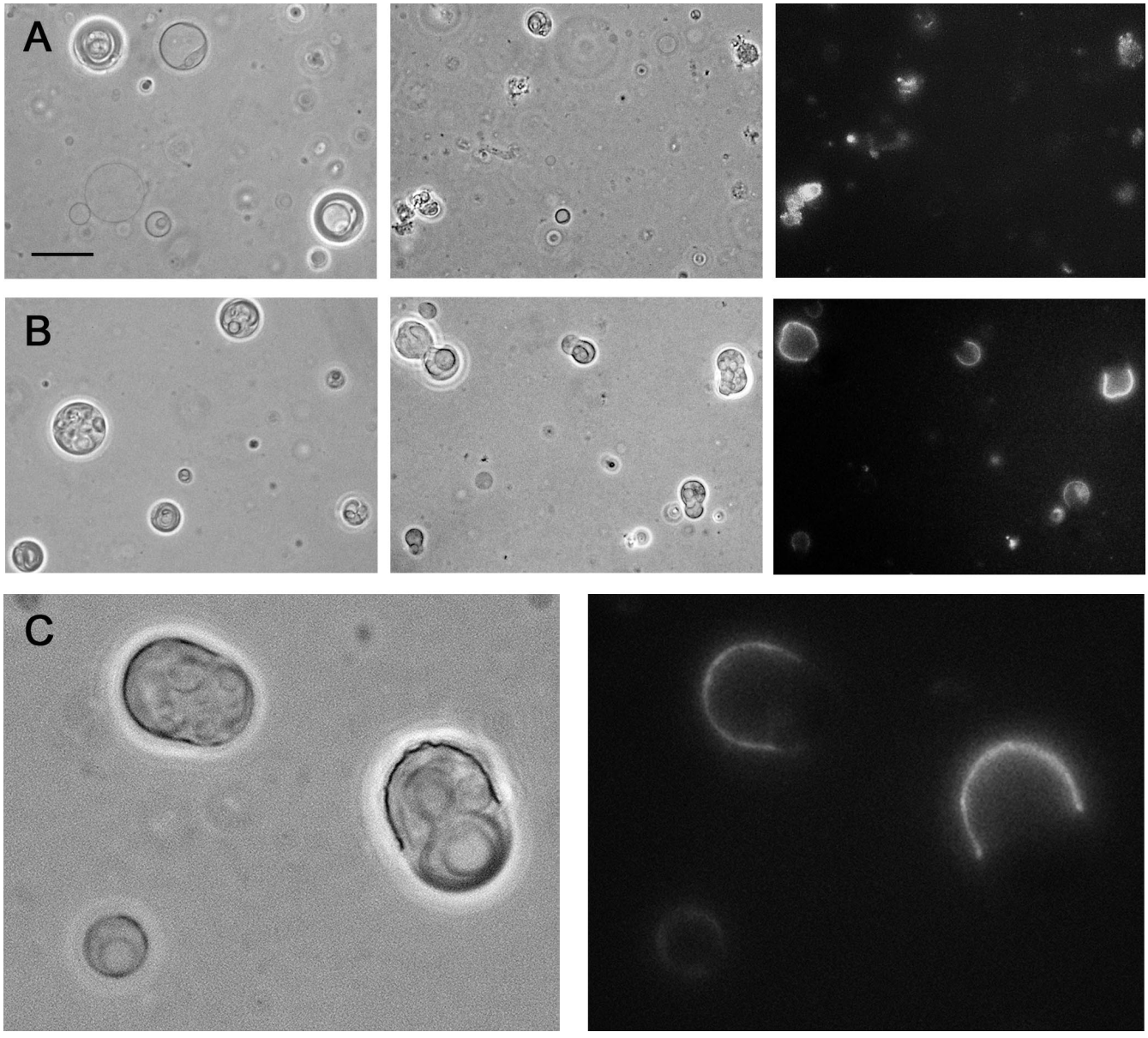

FIGURE 8 Lipid domain formation. The membrane-reorganizing effect of oligonucleotides was visualized by phase contrast and fluorescence microscopy. Giant liposomes in 5 mM citrate buffer were incubated at pH 4 and room temperature with FITC-labeled oligonucleotide (FITC-labeled anti-c-myc) at an oligonucleotide-to-lipid ratio of 0.2 mg/mg in the absence (*A*) and presence (*B* and *C*) of 40% ethanol. Most of the initial giant liposomes were multilamellar and exhibited internal structure (*A, left side*). In the absence of ethanol the giant liposomes fragmented into irregularly shaped structures and smaller liposomes (*A*, phase contrast image in the *center* and the corresponding fluorescence image on the *right side*). In 40% ethanol the initially round liposomes adopted a pear-shaped form after 5–10 min with the oligonucleotide segregated to one side of this structure (horseshoe) (*B*, phase contrast image in the *center* and fluorescence image on the *right side*). Control liposomes in 40% ethanol in the absence of oligonucleotide are shown in *B* (*left side*). An expanded view of MLV in the presence of ethanol and oligonucleotides is presented in *C* (phase contrast image on the *left* and fluorescence image on the *right*). Bar, 20 μm. The magnification is the same for *A* and *B*.

of ethanol also point to an adhesion-mediated process for their formation. However, they differ from the complexes in that they exhibit concentric bilayer shells (Figs. 6 and 10). Although ethanol is required for the latter structures to form, it is not clear how it promotes these structural rearrangements. The ethanol concentrations correlate with the loss of the membrane permeability barrier for small molecules and rapid lipid exchange as well as lipid flip-flop. In addition, ethanol has been shown to reduce the bending rigidity of lipid membranes (Safinya et al., 1989). Permeabilization of the liposomes results in rapid relief of the stress imposed on the lipid membrane by volume loss (water efflux) as the vesicles adhere and flatten against each other. The enhanced lipid exchange as well as the reduced bending rigidity affect

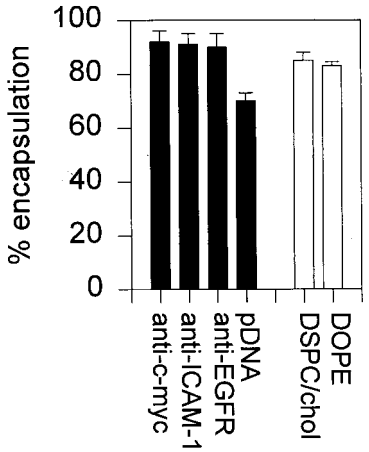

FIGURE 9 (*Solid bars*) Entrapment of different antisense oligonucleotides as well as plasmid DNA (pCMV-luc) in DSPC/Chol/PEG-CerC_{14}/DODAP (20:45:10:25 mol %) liposomes. The initial oligonucleotide-to-lipid weight ratio was 0.1 mg/mg, and 300 mM citrate buffer was used for oligonucleotide entrapment. The pDNA entrapment was performed in 50 mM citrate buffer at a pDNA-to-lipid weight ratio of 0.03 mg/mg. (*Open bars*) Entrapment of anti-c-myc in DSPC/Chol/PEG-CerC_{14}/DODAP (20/45/10/25 mol %) liposomes and DOPE/PEG-CerC_{14}/DODAP (45/10/45 mol %) liposomes. The initial oligonucleotide-to-lipid weight ratio was 0.12 mg/mg for the DSPC/chol system and 0.11 mg/mg for the DOPE system. The initial lipid concentration was 13 mM.

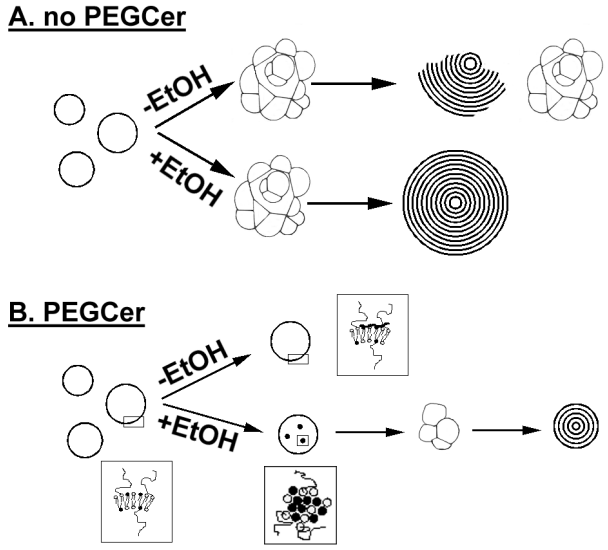

FIGURE 10 Model describing the effect of ethanol and PEG-Cer on the interaction of cationic liposomes with antisense oligonucleotides. In the absence of a PEG coating and ethanol, complexes are formed mainly consisting of aggregates and multilamellar structures with non-concentric membranes (*A, top*). Ethanol induces the formation of large multilamellar liposomes with concentric bilayer shells (*A, bottom*). Incorporation of PEG-Cer prevents aggregation in the absence of ethanol whereas binding of oligonucleotides to the liposomes is not inhibited (*B, top*). Small multilamellar liposomes form in the presence of ethanol preceded by adhesion of the parent LUVs in PEG-Cer-depleted regions (*B, bottom*).

the restructuring of the lipid membranes. It has been shown previously that there is a direct pathway from LUVs to MLVs independent of ethanol (Siegel and Epand, 1997). Similarities with our systems are obvious. At low pH, phosphatidylethanolamine (PE) LUVs, in particular, dipalmitoleoyl-PE (DPoPE) LUVs, aggregate and form small MLVs at temperatures below the lamellar-to-hexagonal phase transition (T_H) (Siegel et al., 1994; Siegel and Epand, 1997). In the case of DPoPE, which has a T_H of 43°C, the extent and rate of MLV formation was temperature dependent, more pronounced at higher temperatures (21°C) with aggregation dominating at lower temperatures (4°C). A similar temperature response was also found for our PEG-Cer-containing liposomes. At low temperature, aggregation was decoupled from subsequent structural reorganizations (Fig. 3). For the PE systems, the formation of concentric bilayer shells was attributed to the large energy of adhesion of PE bilayers at pH 7 or less (Siegel and Epand, 1997).

It is difficult to control the final size of the multilamellar liposomes. With increasing ethanol concentration the entrapment efficiency goes up, but at the same time the size becomes larger and the polydispersity increases (Table 1). Two parameters, among others, that most affect the final size and lamellarity are the oligonucleotide-to-lipid ratio and the ethanol concentration. The former determines the aggregate size and the latter the degree of membrane destabilization. A reduction in size and polydispersity should be possible by limiting the number of adhesion points between liposomes and hence the number of liposomes, which can come into contact with each other. This can be achieved by incorporation of PEG-lipids into the liposome membrane with the polymer concentration being the variable that determines the final size distribution. The polymer coating does not interfere with oligonucleotide binding. Multilamellar liposomes not much larger than the parent LUVs from which they originated formed at PEG-Cer concentrations of 2.5 mol %, and their formation was not inhibited by PEG-Cer concentrations as high as 10 mol %. Adhesion was completely abolished at 10 mol % PEG-Cer in the absence of ethanol. In addition, the PEG coating was shown to prevent structural transformations of cationic liposome/oligonucleotide complexes, resulting in stable adhesion (Meyer et al., 1998). Aggregation was virtually eliminated in the presence of 6 mol % PEG-PE (Meyer et al., 1998).

Ethanol can contribute to liposome adhesion in two ways: first, by the increase in the amount of non-membrane-incorporated PEG-Cer through rapid lipid exchange, and second, by formation of small domains depleted in PEG-Cer and enriched in oligonucleotides. Domain formation was observed with giant liposomes following binding of oligonucleotides in ethanol-containing solutions (Fig. 8). These domains could be regions where contact is established. The spreading of the contact area would lead to lateral displacement and loss of PEG-Cer from the liposome membrane. The latter was demonstrated to occur by the fractionation

studies (Table 2). The subsequent structural rearrangements are again a consequence of this adhesion. It has been shown previously that membrane adhesion is accompanied by lateral phase separation. PEG-PE can be squeezed out from the contact area, thereby allowing growth of adhesion patches (Albersdorfer et al., 1997).

Fig. 10 summarizes how ethanol and PEG-Cer affect the interaction of cationic liposomes with antisense oligonucleotides. In the absence of a PEG coating and ethanol, complexes are formed mainly consisting of aggregates and multilamellar structures with open terminated membranes (Fig. 10 *A*). Ethanol induces the formation of large multilamellar liposomes with concentric bilayer shells (Fig. 10 *A*). In the absence of ethanol, incorporation of PEG-Cer prevents aggregation whereas binding of oligonucleotides to the liposomes is not inhibited (Fig. 10 *B*). Small multilamellar liposomes formed in the presence of ethanol (Fig. 10 *B*). The ethanol concentrations required for their formation were found to be dependent on the lipid composition. Less ethanol was required when liposomes incorporated PE instead of phosphatidylcholine or when PEG-Cer was absent. The effect of oligonucleotide binding will be discussed in the following paragraph.

The binding of highly charged polyelectrolytes to oppositely charged liposomes promotes membrane destabilization per se. Charge neutralization and concomitant reduction of the outer surface area leads to a gradient in lateral pressure in the direction of the bilayer normal. This generates a bending moment, which in turn contributes to destabilize the liposomes (Sackmann, 1994). The severity of the destabilization depends on the polyelectrolyte-to-lipid ratio and ranges from membrane distortion to fragmentation. Membrane distortion as well as invagination were found in LUV systems at high oligonucleotide concentrations or following pDNA binding (Lasic, 1997; Meyer et al., 1998; Xu et al., 1999; May et al., 2000). Exposure of giant liposomes to oligonucleotides and DNA caused budding off of smaller liposomes as well as fragmentation and disintegration (Fig. 8 *A*) (Angelova et al., 1999). Ethanol can enhance the destabilizing effect of oligonucleotide binding. It was hypothesized that invagination and inversion of the liposomal membrane could relieve the resultant stress, provided that there is excess surface area available, and result in entrapment of pDNA in cationic liposomes (Lasic, 1997). This mechanism is not supported by our data. The majority of oligonucleotide is entrapped between the lamellae of multilamellar liposomes. However, it cannot be completely ruled out that it accounts for some of the entrapped antisense in the unilamellar liposomes.

Detergents are able to destabilize lipid membranes in much the same way as ethanol, most notably causing gradual breakdown of the membrane permeability barrier and enhanced lipid exchange (Almog et al., 1990; Schubert et al., 1991). Preliminary experiments show that detergents can be substituted for ethanol. Future work will focus on the characterization of these detergent systems as well as on the general applicability of the ethanol procedure, particularly with respect to the entrapment of positively charged polyelectrolytes in negatively charged liposomes. The limitations imposed by the nature of the polyelectrolyte will be an additional point of investigation. For example, the lack of entrapment of ATP, a small molecule with three negative charges, indicates a dependence on the length of the molecule.

In summary, this study shows that membrane-destabilizing agents can modulate the interaction of cationic liposomes with polyelectrolytes. MLVs form when oligonucleotides interact with cationic LUVs in the presence of ethanol and detergents. Their size can be controlled by incorporation of PEG-Cer. The encapsulation procedure is not restricted to a particular combination of polyelectrolyte and lipid composition but represents a general feature of the interaction of polyelectrolytes with oppositely charged liposomes. The high entrapment efficiencies achieved at high polyelectrolyte-to-lipid ratios and the small size and neutral character of these novel liposomal systems are of utility for liposomal delivery of macromolecular drugs.

We acknowledge Dr. Zhao Wang of Inex Pharmaceuticals for the synthesis of the radioactively labeled PEG-Cer.

This work was supported by the Medical Research Council of Canada and Inex Pharmaceuticals together with the National Science and Engineering Research Council of Canada through a Collaborative Research and Development Program.

REFERENCES

Albersdorfer, A., T. Feder, and E. Sackmann. 1997. Adhesion-induced domain formation by interplay of long-range repulsion and short-range attraction force: a model membrane study. *Biophys. J.* 73:245–257.

Almog, S., B. J. Litman, W. Wimley, J. Cohen, E. J. Wachtel, Y. Barenholz, A. Ben-Shaul, and D. Lichtenberg. 1990. States of aggregation and phase transformations in mixtures of phosphatidylcholine and octyl glucoside. *Biochemistry.* 29:4582–4592.

Angelova, M. I., N. Hristova, and I. Tsoneva. 1999. DNA-induced endocytosis upon local microinjection to giant unilamellar cationic vesicles. *Eur. Biophys. J.* 28:142–150.

Bailey, A. L., and P. R. Cullis. 1994. Modulation of membrane fusion by asymmetric transbilayer distributions of amino lipids. *Biochemistry.* 33:12573–12580.

Barchfeld, G. L., and D. W. Deamer. 1988. Alcohol effects on lipid bilayer permeability to protons and potassium relation to action of general anesthetics. *Biochim. Biophys. Acta.* 944:40–48.

Barry, J. A., and K. Gawrisch. 1995. Direct NMR evidence for ethanol binding to the lipid-water interface of phospholipid bilayers. *Biochemistry.* 33:8082–8088.

Bligh, E. G., and W. J. Dyer. 1959. A rapid method of total lipid extraction and purification. *Can. J. Biochem. Physiol.* 37:911–917.

Chonn, A., and P. R. Cullis. 1998. Recent advances in liposome technologies and their applications for systemic gene delivery. *Adv. Drug Delivery Rev.* 30:73–83.

Duportail, G., and P. Lianos. 1996. Fluorescence probing of vesicles using pyrene and pyrene derivatives. *In* Vesicles. M. Rosoff, editor. Marcel Dekker, New York. 295–366.

Evans, E. A., and V. A. Parsegian. 1983. Energetics of membrane deformation and adhesion in cell and vesicle aggregation. *Ann. N.Y. Acad. Sci.* 416:13–33.

Felgner, P. L. 1997. Nonviral strategies for gene therapy. *Sci. Am.* 276: 102–106.

Felgner, P. L., T. R. Gadek, M. Holm, R. Roman, H. S. Chan, M. Wenz, J. P. Northrop, G. M. Ringold, and H. Danielson. 1987. Lipofection: a highly efficient, lipid-mediated DNA transfection procedure. *Proc. Natl. Acad. Sci. U.S.A.* 84:7413–7417.

Fiske, C. H., and Y. Subbarow. 1925. Colorimetric determination of phosphorus. *J. Biol. Chem.* 66:325–329.

Gao, X., and L. Huang. 1995. Cationic liposome-mediated gene transfer. *Gene Therapy.* 2:710–722.

Gennis, R. B. 1989. Biomembranes: Molecular Structure and Function. Springer Verlag, New York.

Gustafsson, J., G. Arvidson, G. Karlsson, and M. Almgren. 1995. Complexes between cationic liposomes and DNA visualized by cryo-TEM. *Biochim. Biophys. Acta.* 1235:305–312.

Hirschbein, B. L., and K. L. Fearon. 1997. P-31 NMR spectroscopy in oligonucleotide research and development: commentary. *Antisense Nucleic Acid Drug Dev.* 7:55–61.

Hoekstra, D. 1990. Fluorescence assays to monitor membrane fusion: potential application in biliary lipid secretion and vesicle interactions. *Hepatology.* 12:61S–66S.

Holte, L. L., and K. Gawrisch. 1997. Detecting ethanol distribution in phospholipid multilayers with MAS-NOESY Spectra. *Biochemistry.* 36: 4669–4674.

Hope, M. J., Walker, D. C., and P. R. Cullis. 1983. Ca^{2+} and pH induced fusion of small unilamellar vesicles consisting of phosphatidylethanolamine and negatively charged phospholipids: a freeze-fracture study. *Biochem. Biophys. Res. Commun.* 110:15–22.

Huebner, S., B. J. Battersby, R. Grimm, and G. Cevc. 1999. Lipid-DNA complex formation: reorganization and fusion of lipid bilayers in the presence of DNA as observed by cryo-electron microscopy. *Biophys. J.* 76:3158–3166.

Hyatt, M. A. 1981. Principles and Techniques of Electron Microscopy. Edward Arnold Publishers, London.

Kachar, B., N. Fuller, and R. P. Rand. 1986. Morphological responses to calcium-induced interactions of phosphatidylserine-containing vesicles. *Biophys. J.* 50:779–788.

Komatsu, H., and S. Okada. 1996. Ethanol-enhanced permeation of phosphatidylcholine/phosphatidylethanolamine mixed liposomal membranes due to ethanol-induced lateral phase separation. *Biochim. Biophys. Acta.* 1283:73–79.

Koppel, D. E. 1972. Analysis of macromolecular polydispersity in intensity correlation spectroscopy: the method of cumulants. *J. Chem. Phys.* 57:4814–4820.

Lasic, D. D. 1997. Liposomes in Gene Delivery. CRC Press, Boca Raton, FL.

Lasic, D. D., H. Strey, M. C. A. Stuart, R. Podgornik, and P. M. Frederik. 1997. The structure of DNA-liposome complexes. *J. Am. Chem. Soc.* 119:832–833.

Leckband, D. E., C. A. Helm, and J. Israelachvili. 1993. Role of calcium in adhesion and fusion of bilayers. *Biochemistry.* 32:1127–1140.

Lentz, B. R., W. Talbot, J. Lee, and L.-X. Zheng. 1997. Transbilayer lipid redistribution accompanies poly(ethylene glycol) treatment of model membranes but is not induced by fusion. *Biochemistry.* 36:2076–2083.

Lobbecke, L., and G. Cevc. 1995. Effects of short-chain alcohols on the phase behavior and interdigitation of phosphatidylcholine bilayer membranes. *Biochim. Biophys. Acta.* 1237:59–69.

Lipowsky, R. 1991. The conformation of membranes. *Nature.* 349: 475–481.

Macdonald, P. M., K. J. Crowell, C. M. Franzin, P. Mitrakos, and D. J. Semchyschyn. 1998. Polyelectrolyte-induced domains in lipid bilayer membranes: the deuterium NMR perspective. *Biochem. Cell Biol.* 76: 452–464.

Maurer, N., A. Mori, L. Palmer, M. A. Monck, K. W. C. Mok, B. Mui, Q. F. Akhong, and P. R. Cullis. 1999. Lipid-based systems for the intracellular delivery of genetic drugs. *Mol. Membr. Biol.* 16:129–140.

McIntyre, J. C., and R. G. Sleight. 1991. Fluorescence assay for phospholipid membrane asymmetry. *Biochemistry.* 30:11819–11827.

May, S., D. Harris, and A. Ben-Shaul. 2000. The phase behavior of cationic lipid-DNA complexes. *Biophys. J.* 78:1681–1697.

Meyer, O., D. Kirpotin, K. Hong, B. Sternberg, J. W. Park, M. C. Woodle, and D. Papahadjopoulos. 1998. Cationic liposomes coated with polyethylene glycol as carriers for oligonucleotides. *J. Biol. Chem.* 273: 15621–15627.

Miller, D. C., and G. P. Dahl. 1982. Early events in calcium-induced liposome fusion. *Biochim. Biophys. Acta.* 689:165–169.

Mitrakos, P., and P. M. Macdonald. 1996. DNA-induced lateral segregation of cationic amphiphiles in lipid bilayer membranes as detected via ^{2}H NMR. *Biochemistry.* 35:16714–16722.

Mok, K. W. C., and P. R. Cullis. 1997. Structural and fusogenic properties of cationic liposomes in the presence of plasmid DNA. *Biophys. J.* 73:2534–2545.

Needham, D., and E. Evans. 1988. Structure and mechanical properties of giant lipid (DMPC) vesicle bilayers from 20°C below to 10°C above the liquid crystal-crystalline phase transition at 24°C. *Biochemistry.* 27: 8261–8269.

Ostrowsky, N. 1993. Liposome size measurements by photon-correlation spectroscopy. *Chem. Phys. Lipids.* 64:45–56.

Papahadjopoulos, D., and G. Poste. 1975. Calcium-induced phase separation and fusion in phospholipid membranes. *Biophys. J.* 15:945–948.

Papahadjopoulos, D., W. J. Vail, K. Jacobson, and G. Poste. 1975. Cochleate lipid cylinders: formation by fusion of unilamellar lipid vesicles. *Biochim. Biophys. Acta.* 394:483–491.

Radler, J. O., I. Koltover, A. Jamieson, T. Salditt, and C. R. Safinya. 1998. Structure and interfacial aspects of self-assembled cationic lipid-DNA gene carrier complexes. *Langmuir.* 14:4272–4283.

Rand, R. P., B. Kachar, and T. S. Reese. 1985. Dynamic morphology of calcium-induced interactions between phosphatidylserine vesicles. *Biophys. J.* 47:483–489.

Sackmann, E. 1994. Membrane bending energy concept of vesicle- and cell-shapes and shape transitions. *FEBS Lett.* 346:3–16.

Safinya, C. R., E. B. Sirota, D. Roux, and G. S. Smith. 1989. Universality in interacting membranes: the effect of cosurfactants on the interfacial rigidity. *Phys. Rev. Lett.* 62:1134–1137.

Schubert, R., H. Wolburg, K.-H. Schmidt, and H. J. Roth. 1991. Loading of preformed liposomes with high trapping efficiency by detergent-induced formation of transient membrane holes. *Chem. Phys. Lipids.* 58:121–130.

Schwichlenhovel, C., B. Deuticke, and C. W. Haest. 1992. Alcohols produce reversible and irreversible acceleration of phospholipid flip-flop in the human erythrocyte. *Biochim. Biophys. Acta* 1111:35–44.

Semple, S. C., S. K. Klimuk, T. O. Harasym, N. Dos Santos, S. M. Ansell, K. F. Wong, N. Maurer, H. Stark, P. R. Cullis, M. J. Hope, and P. Scherrer. 2001. Efficient encapsulation of antisense oligonucleotides in lipid vesicles using ionizable aminolipids: formation of novel small multilamellar vesicle structures. *Biochim. Biophys. Acta.* 1510:152–166.

Siegel, D. P., and R. M. Epand. 1997. The mechanism of lamellar-to-inverted hexagonal phase transitions in phosphatidylethanolamine: implications for membrane fusion mechanisms. *Biophys. J.* 73:3089–3111.

Siegel, D. P., W. J. Green, and Y. Talmon. 1994. The mechanism of lamellar-to-inverted hexagonal phase transitions: a study using temperature-jump cryotransmission electron microscopy. *Biophys. J.* 66: 402–414.

Slater, S. J., C., Ho, F. J., Taddeo, M. B., Kelly, and C. D., Stubbs. 1993. Contribution of hydrogen bonding to lipid-lipid interactions in membranes and the role of lipid order: effects of cholesterol, increased phospholipid unsaturation, and ethanol. *Biochemistry.* 32:3714–3721.

Slater, J. L., and C.-H. Huang. 1988. Interdigitated bilayer membranes. *Prog. Lipid Res.* 27:325–359.

Struck, D. K., D. Hoekstra, and R. E. Pagano. 1981. Use of resonance energy transfer to monitor membrane fusion. *Biochemistry*. 20: 4093–4099.

Tam, P., M. Monck, D. Lee, O. Ludkovski, E. C. Leng, K. Clow, H. Stark, P. Scherrer, R. W. Graham, and P. R. Cullis. 2000. Stabilized plasmid-lipid particles for systemic gene therapy. *Gene Ther*. In press.

Tocanne, J. F., and J. Teissie. 1990. Ionization of phospholipids and phospholipid-supported interfacial lateral diffusion of protons in membrane model systems. *Biochim. Biophys. Acta.* 1031:111–142.

Vierl, U., L. Lobbecke, N. Nagel, and G. Cevc. 1994. Solute effects on the colloidal and phase behavior of lipid bilayer membranes: ethanol-dipalmitoylphosphatidylcholine mixtures. *Biophys. J.* 67:1067–1079.

Xu, Y., S. W. Hui, P. Frederick, and F. C. Szoka. 1999. Physicochemical characterization and purification of cationic liposomes. *Biophys. J.* 77: 341–353.